Available online at www.sciencedirect.com
SCIENCE DIRECT®
ELSEVIER
Earth and Planetary Science Letters 216 (2003) 109–123
EPSL
www.elsevier.com/locate/epsl

Reconstructing Last Glacial Maximum bottom water salinities from deep-sea sediment pore fluid profiles

Jess F. Adkins [a,*], Daniel P. Schrag [b]

[a] MS 100-23, Division of Geology and Planetary Sciences, Caltech, Pasadena, CA 91125, USA
[b] Department of Earth and Planetary Sciences, Harvard University, Cambridge, MA 02139, USA

Received 31 March 2003; received in revised form 28 August 2003; accepted 5 September 2003

Abstract

Deep-sea sediment pore fluids contain a record of past glaciations in their [Cl] and $\delta^{18}O$. The signal of the Last Glacial Maximum (LGM) ice volume increase remains in the pore fluids as a local peak in each of these species. Using a one-dimensional model to account for the diffusive and advective transport within the sediment column since the LGM, the past bottom water salinity and $\delta^{18}O_{seawater}$ values can be estimated. The model is most sensitive to the shape of the forcing function used to represent bottom water variations through time, the effective diffusion coefficient, and the scatter in the data. Assuming steady-state compaction, the model is relatively insensitive to the initial condition, the bulk sedimentation rate and the assumed porosity profile, though these last two are measured independently. Overall uncertainties in the relative [Cl] increase at the LGM are between 0.1 and 0.5%, where the mean ocean change is about 3.5%.

Keywords: paleo-salinity; diffusion; Last Glacial Maximum

1. Introduction

Measuring the temperature and salinity of the past oceans is an important part of understanding the role of ocean circulation in any past climate regime. Of the two, salinity has proven to be much harder to constrain. Foraminiferal [1,2] and dinoflagellate [3,4] transfer functions and F/Ca [5] ratios in planktonic tests have all been used, with varying degrees of success, to measure the surface ocean salinity in the past. However, until the advent of using pore water [Cl] profiles, no method had successfully established the salinity of Last Glacial Maximum (LGM) deep waters.

In the mid-1980s, McDuff measured a peak in the [Cl] and $\delta^{18}O$ of pore fluids at a sediment depth of 25 m in the Equatorial Pacific [6]. McDuff recognized these peaks as the residual signal of past glaciation modified by advection and diffusion. Using McDuff's data, Schrag and DePaolo [7] showed how a simple one-dimensional diffusion and advection model of pore fluid transport could be used to reconstruct the local LGM $\delta^{18}O$ of bottom water. Recognizing that

* Corresponding author. Tel.: +1-626-395-8550; Fax: +1-626-683-0621.
E-mail address: jess@gps.caltech.edu (J.F. Adkins).

0012-821X/03/$ – see front matter © 2003 Elsevier B.V. All rights reserved.
doi:10.1016/S0012-821X(03)00502-8

better data were needed, Schrag et al. measured $\delta^{18}O$ at high precision and high depth resolution in the Equatorial Atlantic [8]. These data suggested a much smaller change in $\delta^{18}O$ due to continental ice sheets than previously thought [9]. These results have been confirmed with more cores and indicate that deep-ocean temperatures were near the freezing point at the LGM [10].

Using an analytical method borrowed from McDuff, Adkins and Schrag made the first combined measurements of LGM $\delta^{18}O_{water}$ and salinity [11]. Bottom water salinity in the North Atlantic at the Bermuda rise was found to be much fresher than the assumed mean 3.2% increase based on 125 m of eustatic sea-level change. In principle the combined $\delta^{18}O_{seawater}$ and [Cl] estimates can be combined with benthic foraminiferal $\delta^{18}O$ at the same site to constrain the temperature and salinity of deep-water masses at the LGM. Based on several Ocean Drilling Program (ODP) cores from a wide variety of sites, Adkins et al. used this technique to make a glacial *T*/*S* plot for the abyssal ocean [12]. This result demonstrates a fundamental change in the stratification of the LGM relative to the modern ocean. As most of the glacial deep ocean was cold and nearly isothermal, salinity rather than temperature determined the density differences in the deep waters. However, the results of this analysis are dependent on a careful understanding of the contributions of both data and model sensitivities to the final result. In this paper we concentrate on the behavior of [Cl] in one-dimensional pore fluid models, exploring the sensitivity to a wide range of parameters. Although the sensitivity tests discussed here are specifically formulated for chloride ions, the results share many features with models of $\delta^{18}O$ as well.

2. Methods

2.1. Measuring chloride at high precision in pore fluids

We use the standard methods of the Ocean Drilling Program [13] to recover pore fluids from sediments. Whole rounds are cleaned of mud that contacted drilling fluid and are pressed in the standard 'Mannheim' squeezer. Once removed from the sediment, pore waters are filtered through 53 μm GFF filters and heat-sealed in glass ampoules or sealed in screw top glass vials with plastic insert tops and parafilm. Samples stored in vials at sea are transferred to glass ampoules immediately after they are received in our shore-based lab.

Chloride ion concentrations are determined by potentiometric titration of 750 μl of pore water against a silver nitrate standard. Values are reported as g/kg to avoid measuring the in situ pore fluid density for each sample. Unlike bulk salinity, which is altered by the reduction of sulfate in pore fluids, chloride concentration is conservative in both the open ocean and the sediments (except in regions of clathrate formation) and is therefore the best measure of past salt variations. The measurement procedure follows the pioneering work of Gieskes [13] and modifications made at Caltech. The chief improvement over the earlier method is the use of a home-built autotitrator. All samples and IAPSO standards are diluted with approximately 5 ml of deionized water after weighing in a small beaker containing a magnetic stir bar. Using a microburette fitted with a silver wire passed through the wall of the main reservoir, the potential difference across the silver nitrate solution and the sample is monitored with a voltmeter (Fig. 1). After adding approximately 99% of the $AgNO_3$ needed to reach the end point, silver chloride precipitates are 'aged' for 5 min to release Ag ions trapped in their pore spaces. It is important to make measurements at regular time intervals after this step to reduce the effects of voltmeter drift and diffusion of $AgNO_3$ from the burette tip into the sample solution.

Standard concentrations, generally around 0.2 M [Ag], are calculated from titrations with an IAPSO solution of known salinity. Standards are measured in triplicate at the beginning of each day and occasionally checked at day's end. Over the course of a month, the typical lifetime of an individual batch of standard, the silver nitrate concentration drifts by less than 3 parts in 2000. I and Br species will also precipitate as their re-

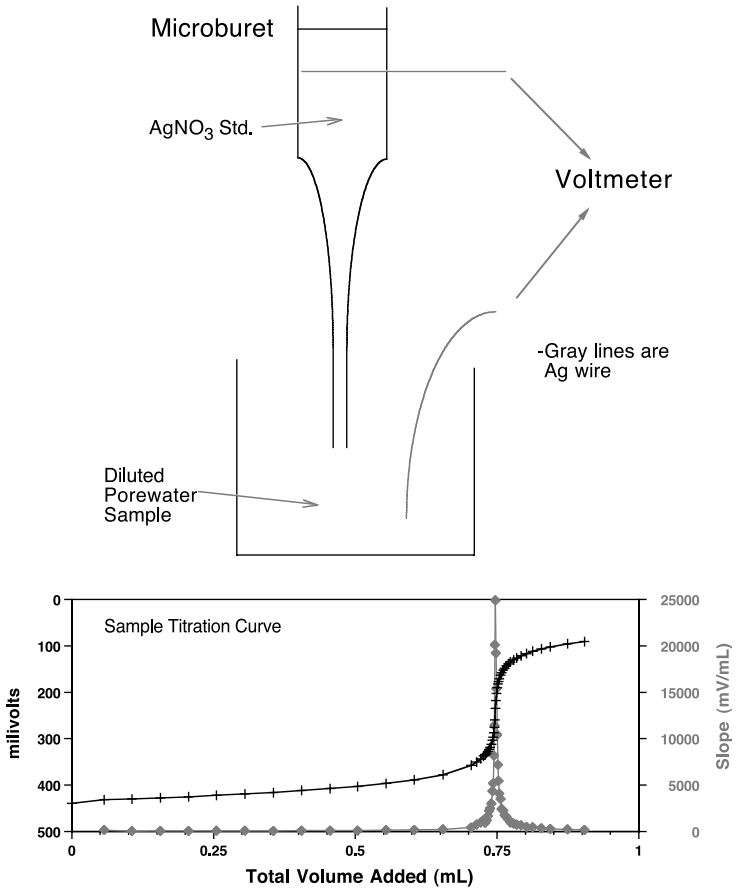

Fig. 1. Schematic of the automated potentiometric titration of chloride ion with silver nitrate. A diluted 750 μl sample of pore fluid is titrated against an $AgNO_3$ solution that has previously been calibrated with IAPSO. The end-point is determined by monitoring the electrical potential between the sample solution and the pure standard in the microburette. As the added Ag^+ is consumed by free Cl^- from the sample there is a large buffer region where the potential is large and invariant (black line with black crosses). Once the last Cl^- is consumed, added Ag^+ leads to a large decrease in the measured voltage. The first derivative of this curve (gray line with gray diamonds) is a sensitive indicator of the titration end-point.

spective silver salts, but concentrations are very low in deep-sea pore fluids.

2.2. Pore fluid modeling

Pore fluid profiles are modeled using the one-dimensional diffusion/advection tracer equation:

$$\phi\frac{\partial C}{\partial t} = \frac{\partial}{\partial z}\phi D\frac{\partial C}{\partial z} - \phi\omega\frac{\partial C}{\partial z} + Rxn \qquad (1)$$

where C is the concentration of the tracer, t is time and z is depth below the sediment–water interface (positive downward). While there is evidence for water exchange with clay minerals at depth in the sediment (see below), our model assumes the reaction term (Rxn) is zero. Where this is not the case in the deep part of the profile, we alter the initial condition to simulate the effects of reaction on the LGM pore water maximum. The diffusion coefficient (D) is temperature- and tortuosity-dependent [14]. Porosity (ϕ) and temperature profiles for each site are taken from the ODP Janus database (www.oceandrilling.org) and tortuosity is modeled as $1-2\ln(\phi)$ [14]. Using

these profiles, the history of bulk sedimentation rate and the assumption of steady-state compaction [15], the fluid advection is given by:

$$\omega = \omega_0 \frac{\phi_0}{\phi} \tag{2}$$

$$\omega_0 = W_0 \frac{\phi_x}{\phi_0} \frac{(1-\phi_0)}{(1-\phi_x)} \tag{3}$$

At any time step the fluid advection vertically within the sediment (ω) is related to the advection at the sediment–water interface (ω_0) by the porosity profile and the instantaneous bulk sedimentation rate (W_0). This equation assumes that the only fluid movement, outside of diffusion, is due to compaction of the sediment. This steady-state compaction assumes that there is a depth (x) where porosity does not change (ϕ_x). We do not include the effects of imposed fluid flow from temperature or pressure gradients in the sediments. The MATLAB code is centered space and forward time with upwind difference for advection. A gradient bottom boundary is used at the deepest points because sediment is passed out of the model domain as the sediment–water interface (always the zero point) moves upward.

A history of the top boundary condition, the concentration versus time plot of the sediment–water interface, is the forcing we vary to fit the measured profile. We have important constraints on the shape of this history and use the model to fit the amplitude of the switch from glacial to modern conditions. Given this construction, the model must be passed several arrays: depth profiles of porosity, initial tracer concentration, and the temperature dependence of D, as well as the time history of the sedimentation rate. Data for all of these parameters, except for the initial condition, are taken from shipboard data as recorded in the ODP database. Sensitivities of the model results to many of these parameters are calculated and discussed below.

3. Results

Given weighing errors and a consistent delivery volume of 0.003 ml, the theoretical uncertainty on any single measurement is about 0.04%. Our replicate precision comes close to matching this propagated error, averaging around 0.05% (Fig. 2A). There was a step change in the consistency standard in November 2000 because of a change in the bottle's storage container (Fig. 2B). On days where the precision exceeds 0.1% we do not continue to run samples.

We find three characteristic deep-ocean [Cl] profile shapes (Fig. 3). In all cases the top of the profile at the sediment–water interface is within error of the bottom water value estimated from modern hydrography. In many cases there is significant structure in the upper 20 m of the profile. In all cases, the upper portion of the profile does not track the model-predicted curve based on known sea-level histories for the Holocene. These upper profile features represent a particular site's response to changes in the global salinity since the

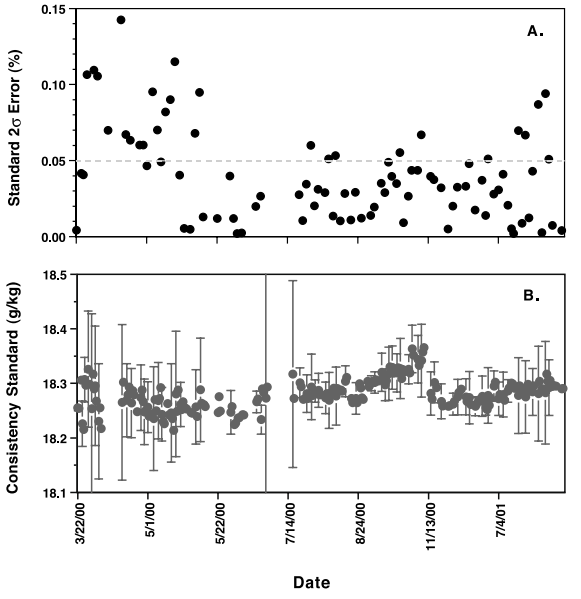

Fig. 2. Reproducibility of the measurement from a surface ocean salinity sample. Water from the Long Marine Lab (Santa Cruz, CA, USA) was measured in triplicate every day we measured pore water samples. (A) 2σ error of the triplicate measurements versus date run. After an initial learning period, we consistently achieved ±0.05% precision or better. (B) Absolute value of the consistency standard over the same time period as in panel A. There was a clear jump in concentration in November of 2000 due to a change in the storage container.

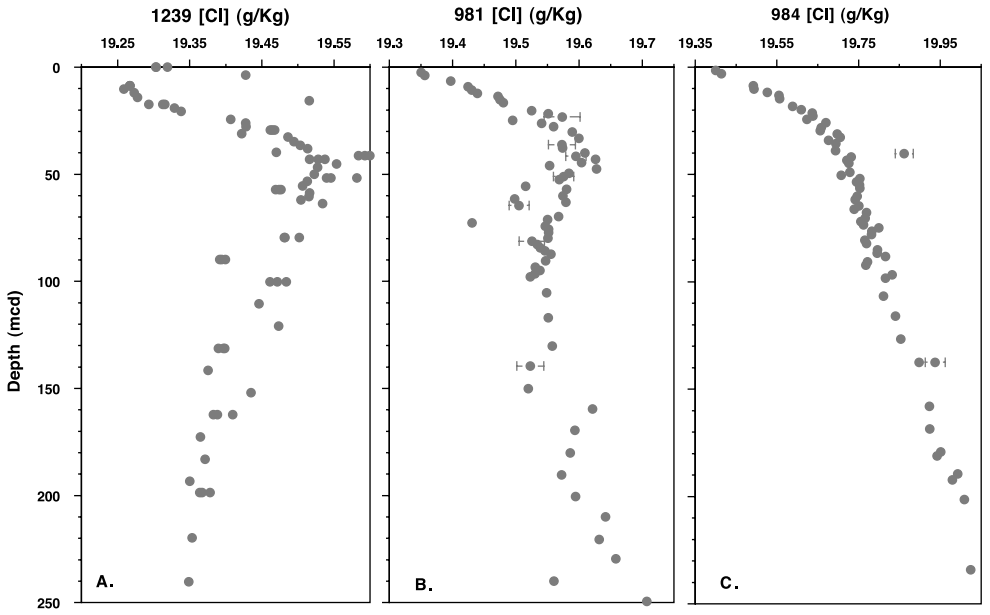

Fig. 3. Three typical profiles of [Cl] in the upper 250 m of deep-sea pore fluids. (A) Typical profile from the Equatorial Pacific (ODP Leg 202, Site 1239). There are some evaporated points in the upper portion of the profile (confirmed by elevated $\delta^{18}O$ in the same samples) that are probably due to collection at sea. The data have the typical profile of bottom water values at the top; a maximum at several 10s of meters depth and a turn around to lower values as the bottom of the profile that 'feels' the basalt–sediment interface. (B) Typical intermediate [Cl] profile that still leads to reliable estimations of glacial bottom water salinity. There is still a discernable subsurface maximum with a turn to fresher values at depth. The deepest portions show an increase in [Cl] as smectite formation takes up water molecules. (C) Typical profile that does not constrain bottom water salinity at the LGM. Here water uptake by clay minerals has overwritten the glacial signal of increased salinity.

LGM. We will not concentrate on these features in this paper but instead limit our discussion to the LGM salinity signal contained in our measured profiles.

A 'standard' profile, represented by Equatorial Pacific Site 1239 in Fig. 3A, has a concentration peak corresponding to the LGM in the upper 40 m. Below this feature the profile gets progressively less concentrated for either the rest of the core or until methane clathrates are encountered. At a small number of sites, we have recovered profiles where there is a change in slope associated with the LGM, but the profile is always increasing with depth. North Atlantic Site 984 (Fig. 3C) was drilled near Iceland and shows the continuously increasing behavior characteristic of sites near large volcanic centers. As has been discussed by other authors [16], this feature is probably due to the conversion of fresh volcanic ash to hydrated clay minerals. In these profiles, as clay minerals swell with waters of hydration, chloride ion is still conservative but water is not. This ash diagenesis overwhelms the glacial–interglacial signal in [Cl] and makes these sites pore constraints for LGM salinity. Finally, several of the sites show an intermediate behavior between these two extremes where the LGM peak is defined but concentrations at depth continue to increase after an initial turn towards fresher values (Fig. 3B). Here there is evidence for ash conversion but it is not large enough to have erased the glacial–interglacial signal we attempt to model in the next section.

4. Model sensitivities

Given the number of arrays that must be passed to the 1-D diffusion/advection model, our final result for the salinity of LGM bottom water at a given site could have many sources of uncertainty. However, in this section we will demonstrate that the three most important parameters

are the shape and amplitude of bottom water boundary condition and the value of the effective diffusivity. For two of these three variables we have strong independent constraints. The third, the glacial–interglacial amplitude of bottom water salinity, is the result we are attempting to model.

4.1. Sedimentation rate and porosity

Together, the bulk sediment accumulation rate and the porosity profile set the pore water advection term. Because the Peclet number for all of our sites and sediment depths ranges between 0.03 and 0.06, we do not expect there to be a large sensitivity to the model's advection scheme. Where porosity is decreasing, the bulk sediment is buried faster than the pore water relative to the sediment–water interface (see Eqs. 2 and 3 above). This appears, in the reference frame of a single layer, as an upward movement of fluid, but it does not mean that fluid is being pushed out the top of the sediment column. New porosity, added as the next layer of sediment is added, balances this apparent 'upward' movement of fluid and correctly models the addition of bottom water to the sediment column. For a standard pore water profile, where [Cl] decreases after the LGM peak, this advection works to dampen the in situ chloride ion maximum and larger sedimentation rates, for the same porosity profile, will increase this advective dampening affect. However, larger sedimentation rates also increase the diffusion path length and lead to larger in situ maxima.

The model's sensitivity to bulk sedimentation rate variation is shown in Fig. 4. We used a sediment column initial condition of constant [Cl] (19.30 g/kg). Porosities from Site 1063 were used in this test, but substituting other sites does not change the fundamental result. In general our final calculated salinities are not sensitive to the model porosity profile because the shipboard data (GRAPE and individual calibration points) are comprehensive and accurate, and they allow us to prescribe the correct profile for each site a priori. The model sediment column in Fig. 4 was forced with constant bottom water [Cl] of 19.30 g/kg, except for a 1000-yr long square wave of 20.30 g/kg from 20 000 to 19 000 yr BP. The resulting pore water profile at 0 yr BP for one run is shown

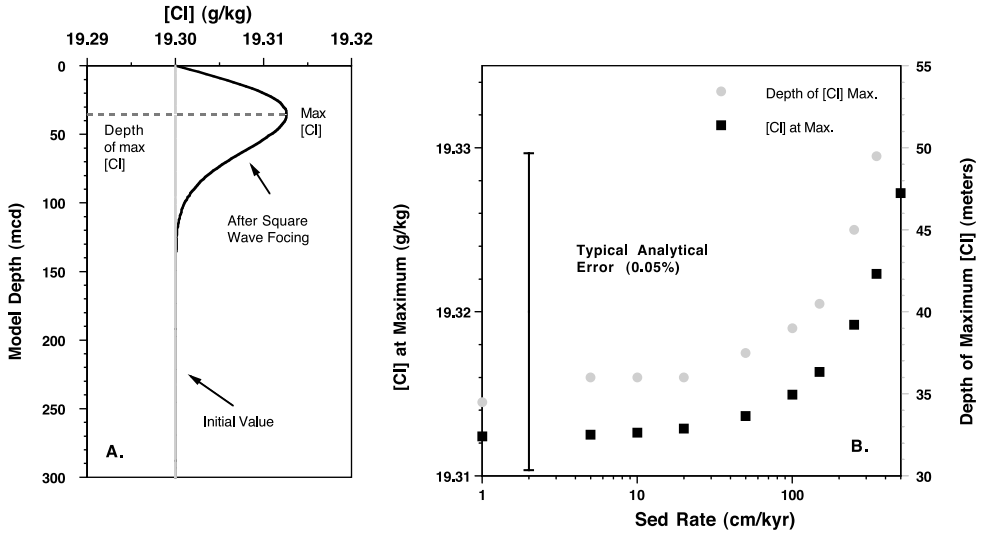

Fig. 4. Sensitivity test of sedimentation rate on the modeled LGM salinity. (A) Shape of the initial condition (gray line) and final profile (black line) after forcing with a square wave of 20.3 g/kg for 1000 yr, 20 000 yr ago. The sediment depth and [Cl] at the maximum value are indicated. (B) Results of varying the sedimentation rate from 1 to 500 cm/kyr. Black squares show that over this huge range of sedimentation rates the [Cl] changes are smaller than our analytical error. Gray circles indicate that the depth of the chloride maximum can be driven about 15 m deeper over this $>10^2$ range in deposition rate.

in Fig. 4A. We altered the bulk sedimentation rate from 1 to 500 cm/kyr, ran the model, and recorded the maximum [Cl] in the profile and the depth of this maximum value. As expected, both the maximum value and the depth of this peak increased over the 500-fold range in sedimentation rate. However, the range in [Cl], ~0.016 g/kg, is smaller than our analytical error for a single point, 0.019 g/kg. Because we have independent constraints for sedimentation rate from the core's age model, which are much better than a factor of 500, our modeled [Cl] results are insensitive to this parameter. The depth of the modeled chloride maximum does change by about 15 m in this test. Without the independent information about sedimentation rate from the core's age model, this deepening of the profile could be seen as a decrease in the effective diffusivity and therefore affect the modeled LGM salinity (see below).

4.2. The initial condition and imposed advection

As with any time-dependent model, there is a chance that our choice of initial condition for the sediment column could affect the final result. This effect is necessary and expected in the deeper portions of the profile, but is largely unimportant for the region around the [Cl] maximum up to the sediment–water interface. This fact follows from the basics of diffusion. For a model run of 125 000 yr and an effective diffusivity of 5×10^{-6} cm^2/s, the diffusive length scale is about 44 m. Including both the sediment added over this time period and the effects of compaction advection pushes the depth of sediment that 'feels' the effects of changes at the sediment–water interface to about 100 m. This effect can be visualized by following several time slices of a typical model run from its initial condition 125 000 yr ago to the final profile we would measure today (Fig. 5). From these 25 000-yr time steps it is clear that the upper 50 m of sediment experiences large variations in [Cl] due to the shape and amplitude of the bottom water forcing function. In its upper portion the final profile has no 'memory' of the initial condition. While this is true for the upper portions of all our measured profiles, there is clearly different

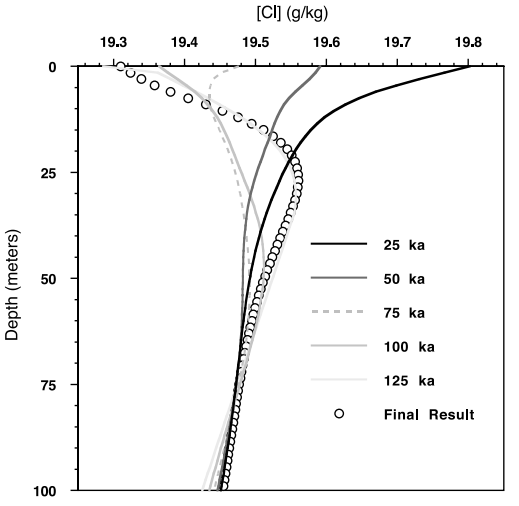

Fig. 5. Model evolution over 125 000 yr. The initial condition (125-ka gray line) is very similar to the final result (black circles) for the given forcing amplitude with a slight increase in the total Cl content. Between these two times the profile gets progressively saltier as the glacial ice sheet increases in volume. At 25 ka (thick black line) the profile and bottom waters are both near maximum [Cl]. During the deglaciation there is a rapid flip of the upper portion of the profile as bottom waters are diluted by rapid deglaciation.

behavior at depth in the sediment that requires separate approaches to initial conditions.

For the standard profiles, where [Cl] decreases with depth after the LGM peak, we establish an initial condition by forcing the sediment column with 3.51 Ma of bottom water [Cl] variability. Starting with constant [Cl] in the sediment column, we force the top boundary with a scaled benthic δ^{18}O record from ODP Site 659 [17]. Using Site 1239 as an example and assuming a 4.0% change in bottom water salinity from the LGM to today as a scaling factor gives the black line shown in Fig. 6. This line is then used as the initial condition in the standard 125 000-yr runs. We repeat this process for each site, changing the glacial [Cl] amplitude and diffusion coefficient as appropriate.

For these 'normal' profiles (see Fig. 3A), we can test the sensitivity of the model's shape at depth in the sediment to our assumption of zero imposed pore fluid flow. Keeping the same 4.0% scaling and adding 0.01 cm/yr of flow to Site 1239 changes the curvature in the lower portion

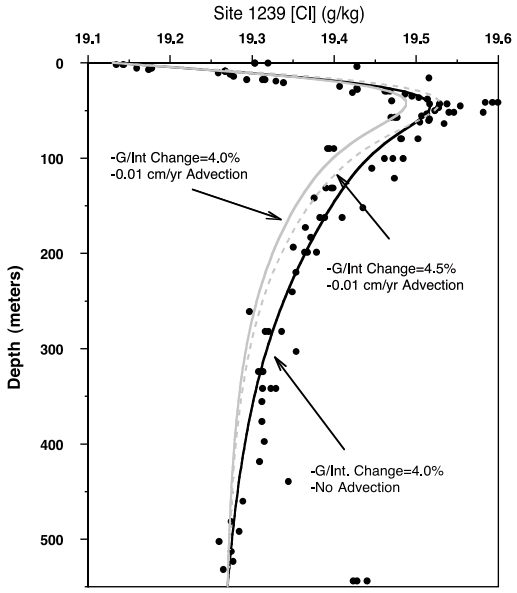

Fig. 6. Effect of imposed advection on the modeled pore fluid profile. Data (black circles) are from Site 1239 in the Equatorial Pacific. An initially constant pore fluid profile was forced with 3.51 Ma of sea-level change based on ODP Site 659. The result with only compaction-driven advection fits the deepest portions of the profile very well. Adding a constant imposed advection (i.e. from pressure or temperature gradients in the sediment) of 0.01 cm/yr (gray lines) pushes the model profile off of the data at depth. Regardless of the model's glacial–interglacial amplitude, there is too much curvature in the cases with imposed advection.

of the profile (solid gray line in Fig. 6). Correcting the misfit at the LGM peak by increasing the scaling to 4.5% still preserves the incorrect curvature at depth (dashed gray line in Fig. 6). As has been demonstrated previously for pore water profiles of $\delta^{18}O$ [7,8], the deeper portions of the data are a strong constraint on the range of possible imposed advection values.

For profiles that do not continuously decrease with depth below the LGM maximum, we must change our modeling approach to fit the lower portions of the profile. The ideal solution is to add a reaction term to the model equations to simulate the uptake of water by ash diagenesis and then run for 3.51 Ma using the same bottom water forcing as above. However, this approach introduces a suite of new variables (water uptake reaction rate, the rate of ash addition through time, diffusion-limited ash diagenesis and the reaction mechanism in general) that are not related glacial bottom water salinities and do not affect the LGM results we are interested in here. For altering the initial condition at depth not to affect our LGM results, the two processes, salt flux from the bottom water boundary and salt flux from water uptake into clay minerals, must be separable in space. In profiles that continually increase with depth this is clearly not the case. For 'intermediate' profiles the ash diagenesis flux has not been able to alter the signal from glaciation. It might appear that chloride added at depth must also be added in the LGM peak region, but in intermediate profiles this flux is too small to matter. To support the observed slope of [Cl] versus depth at Site 1093 the reaction flux need only be $\sim 5\times10^{-9}$ g Cl/(kg yr). This is clearly not large enough to affect the signal from bottom water salinity change since the LGM. These sites can be successfully modeled because at the depth of the LGM maximum the flux of chloride ion from ash diagenesis is small compared to the flux from changes in the bottom water [Cl]. True peaks in the [Cl] profile demonstrate that in situ fluxes are small and the two processes, LGM bottom water salinity changes and reactions within the sediments, are separable within the sediment column.

However, an in situ increase in [Cl] in these intermediate profiles can affect the modeled LGM salinity indirectly because this reaction flux will change the slope of [Cl] versus depth just below the LGM pore water peak. These 'intermediate' profiles can be divided into three regions: the deglacial portion above the LGM [Cl] peak, the deepest portion where [Cl] continuously increases, and the middle portion between the LGM peak and the turn towards higher values (Fig. 7B). As described above, the upper portion is mostly influenced by the imposed bottom water boundary condition (see Fig. 5) and the lowest portion has no effect on the LGM peak. The middle portion, on the other hand, can have some effect on the modeled [Cl] peak because the diffusion operator depends on the gradient in the [Cl] slope. So, the steeper the [Cl] slope in the middle portion of the profile, the smaller (and shallower) the chloride peak. This effect is dem-

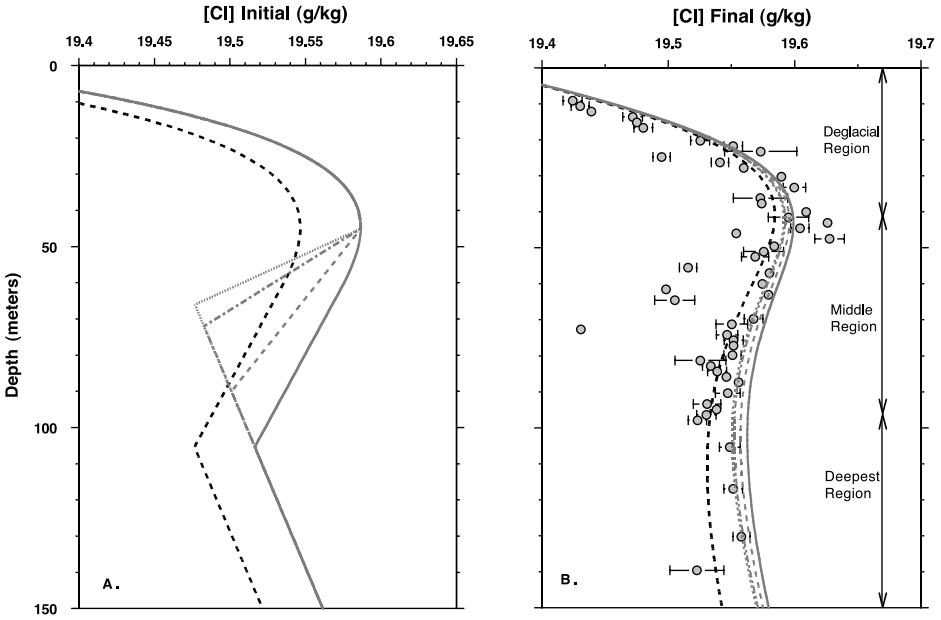

Fig. 7. Effect of a 'kink' or 'turn back' in the measured chloride profile on modeled LGM bottom water salinity. (A) Several different initial conditions used to model the effects of increasing [Cl] at depth in the profile but retaining a turn towards fresher values just below the LGM peak. Gray lines represent various slopes and depths of the 'kink'. The black line represents an overall lowering of the salt content of the sediment initial condition. (B) Resulting profiles from the initial conditions in panel A. The maximum chloride concentrations for all gray-line initial conditions are within analytical error of each other. The largest effect is for the lower overall salinity content of the sediment, but we have strong constraints on this value from the deeper part of the profile.

onstrated for a variety of middle portion slopes in Fig. 7. A family of possible slopes for Site 981 is shown in Fig. 7A and their resulting final profiles after 125 000 model years are shown in Fig. 7B. A wide range of initial slopes leads to relatively small changes in the modeled [Cl] at the LGM peak. The differences in the model profiles at maximum [Cl] in Fig. 7B are much smaller than the analytical error in chloride.

Our model results at the LGM peak are sensitive to the initial absolute value of [Cl] at depth in the sediment (dashed black line in Fig. 7, where we have lowered all initial [Cl] values). This result is simply due to the overall lower chloride ion content of the pore water column in the dashed black line case. These lower [Cl] values 'pull' the same bottom water boundary forcing to an overall lower peak [Cl]. The effect is analogous to the standard profile case where the shape of the profile at depth is a strong constraint for the model's initial condition. For these 'intermediate' type profiles, large amounts of scatter in the deeper profile can therefore lead to larger uncertainties in LGM salinity through its uncertainty in the initial condition. However, Site 981 is an extreme case (see Fig. 3) and the different model peaks are still within the uncertainty of the analytical error bars. The measured modern profile is a good first guess at an initial condition for the model. Changes in the [Cl] slopes at depth, simulating different in situ inputs of chloride, have little effect on the final LGM salinity.

4.3. The shape of the bottom boundary condition

From Fig. 5 it is clear that the shape of the bottom water boundary condition has a first-order effect on the modeled pore fluid profile. We construct our 125 000 yr of bottom water history from a Pacific benthic $\delta^{18}O$ record (V19-30) [18]

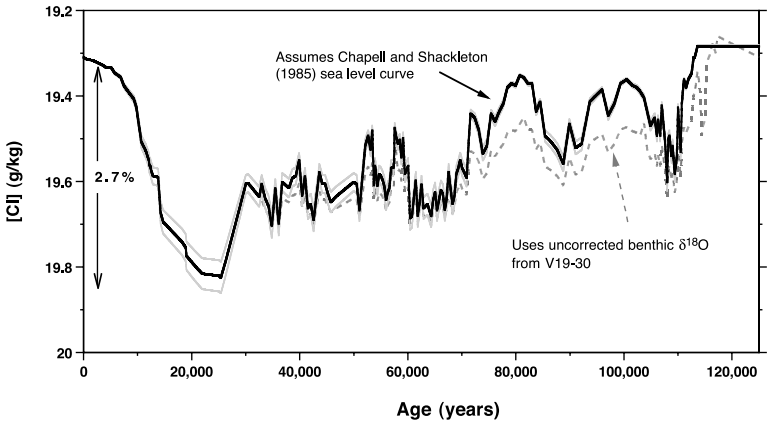

Fig. 8. Shape of the bottom water boundary condition, the chief forcing of the pore fluid model. Solid lines are a combination of the coral sea-level data for the last 30 000 yr and the deep-water temperature record of Chapell and Shackleton. Gray solid lines are the 0.3% deviation from the black line's glacial–interglacial amplitude of 2.7%. The dashed gray line scales [Cl] to the benthic $\delta^{18}O$ record of V19-30 uncorrected for the effects of bottom water temperature change. This incorrect forcing shape exposes the pore fluid to salty bottom waters about 40 000 yr earlier than the more realistic black solid line.

and the coral record of sea-level history for the past 30 000 yr [19,20]. In addition, we follow the work of Chappel and Shackleton [21] to subtract out the competing effect of temperature variability from the sea-level signal in benthic $\delta^{18}O$. This change assumes that all of the deep-water cooling happens at the isotopic stage 5e/5d transition and that all of the deep-water warming occurs at the isotopic stage 2/1 transition. The altered benthic and coral records are then scaled to represent [Cl] variability as shown in Fig. 8. At the maximum sea-level lowering implied by the corals we assign our maximum percentage increase in local chloride concentration. For the black line in Fig. 8 this [Cl] increase is 2.7% greater than the modern bottom water value of 19.31 g/kg. For the same shape of the bottom water history, different LGM–modern amplitudes are imposed above and below a best-fit increase (gray lines in Fig. 8). For a sediment column equivalent to Site 1063 the resulting model pore water profile is the black line in Fig. 9. If we did not subtract the effect of bottom water temperature from the benthic $\delta^{18}O$ values the shape of our bottom water [Cl] would be the gray dashed line in Fig. 8. This curve increases the mean bottom water [Cl] at about 110 000 yr ago, or about 40 000 yr before the correctly adjusted curve. Exposing the sediment column to saltier waters for a longer

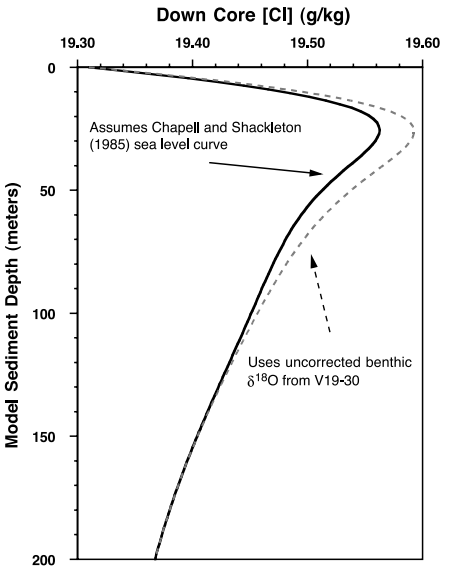

Fig. 9. Model results for the two different shapes of Fig. 8 and a glacial–interglacial amplitude of 2.7%. The uncorrected curve is clearly saltier and has a greater [Cl] at the LGM peak. These features are due to the much longer exposure of pore fluids to salty bottom waters in the case where the temperature effect on benthic $\delta^{18}O$ is not accounted for. The difference between these two curves represents about 0.3% in the absolute value of reconstructed LGM bottom water [Cl]. However, profiles fit with the incorrect forcing would still have the correct relative salinity changes.

period of time pushes more chloride into the model profile and leads to larger modeled [Cl] peaks for the same amplitude of the forcing function (dashed gray line in Fig. 9). In our first work on Site 1063 [11] we did not use the corrected curve and reported an LGM salinity that was about 0.2% too high (which is an 8% larger model amplitude). For our latest compilation of pore fluid profiles [12] we corrected this oversight.

4.4. Effective diffusivity

The diffusion coefficient for chloride ion in seawater is about 1.18×10^{-5} cm^2/s at 5°C [22]. However, electrical gradients, bioturbation and other unmodeled processes, in addition to the porosity, tortuosity and temperature effects that we do consider, lead to differences in sediment diffusivity from this open ocean number. To account for this variation, we assign a separate diffusion coefficient for each of our sites by exploiting the fact that the distance a diffusive process will move material is independent of the size of the forcing. So, we can use the depth of the [Cl] peak to constrain D_{eff} and then use the measured amplitude and D_{eff} to determine the bottom water salinity at the LGM. This calculation assumes that we have accounted for all of the non-diffusive influences (described above) on the depth of the [Cl] peak. Analytical errors and general scatter in our profiles both lead to uncertainty in D_{eff} and therefore directly to uncertainty in LGM salinities. These effects in Site 1063 are shown in Fig. 10. A best-fit D_{eff} is 2.9×10^{-6} cm^2/s (black line). Keeping everything else about the model the same, this value has been increased by 120 and 150% for the gray lines and decreased by 50 and 70% for the gray dashed lines. Given the anomalously low [Cl] at 25 m both the 120 and 70% changes are still reasonable fits to the data. For D_{eff} values that are too low, the shallow points at 20 and 15 m are too far from the model curve. For D_{eff} values that are too high the model peak falls below these two data points. In general we find that scatter in the profiles leads to about a 30% uncertainty in D_{eff} and a 0.1–0.3% uncertainty in the LGM salinities. These errors are included in our reported values.

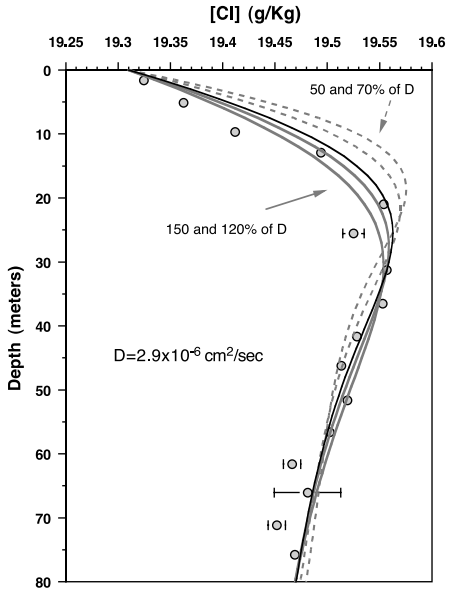

Fig. 10. Effect of the effective diffusion coefficient on model fits. D_{eff} can vary by about ±20% for any given profile before the depth of the [Cl] maximum does not match the data. This variation in D_{eff} is included in our estimates of LGM bottom water [Cl] uncertainty.

5. Discussion

5.1. Overall uncertainty in salinity reconstruction

The overall effect of the model sensitivities enumerated above is to impart a quantifiable level of uncertainty to the LGM salinity from each measured deep-sea pore fluid profile. The largest sources of error are the value of D_{eff}, the scatter of the data points in the profile, and the shape of the bottom water boundary condition. However, this last effect has an interesting feedback with the choice of D_{eff}. The modeled profile is sensitive to the timing of the glacial maximum. Moving the LGM peak of the forcing function back in time deepens the modeled pore fluid peak and would seem to require a larger glacial–interglacial amplitude to fit the data. Both of these features arise from the longer time the model has to diffuse away the LGM signal. But the implied larger amplitude from the model is actually offset by the decreased D_{eff} needed to match the model depth with the data. A smaller D_{eff} means that a smaller model forcing is necessary to fit the measured

profile because the signal does not diffuse away as rapidly. These two effects compensate for each other and the result is a reconstructed LGM bottom water salinity that is very similar for both the early and the late LGM scenarios. This balance between D_{eff} and the modeled amplitude also holds true for profiles of $\delta^{18}O$ [10].

Three previously published pore water profiles can demonstrate how the largest sources of error translate into an overall uncertainty in the LGM bottom water salinity (Fig. 11). These three profiles were all used to generate the *T*/*S* plot for the LGM [12], they have different levels of scatter in the data and they have different D_{eff}s in their models. Profiles are ordered from least precise to most certain in Fig. 11. The largest absolute uncertainty is at Site 1093, but this is also the Southern Ocean location with the largest glacial–interglacial salinity change. Site 981 (Fig. 11, left) has a large degree of scatter in the samples, which translates into about a 10% relative uncertainty. Individual points with low [Cl] like the one at 72 m are clearly artifacts from sampling because there is no way a diffusive water column could retain such a large gradient in salinity over 1.5 m. This profile was measured at Caltech long after the cruise collected the pore fluids. The ~5-yr time lag is probably the largest source of [Cl] change.

In contrast to Site 981, Site 1123 has a very tight profile in the upper and lower portions, outside of some clear low [Cl] fliers. This coherence leads to a relative uncertainty of about 5%. However, at the LGM peak there is a decision to be made. Gray lines in Fig. 11 (right) represent ±0.2% changes in the model's glacial–interglacial amplitude. We could have fit a family of lines through the fresher points at the LGM peak and reported a smaller salinity, but this strategy would leave the data around 20 m too salty. In this case, the sampling at sea would have had to evaporate some samples and freshen others. We choose to model the saltiest points and assume that there was a slight problem with drying the squeezers in-between samples on this cruise. As we have recently collected some Equatorial Pacific profiles (Leg 202) that also show at least a 4% increase in the LGM salinity (J.F.A., unpublished data), this choice seems to have been the correct one.

Relative uncertainty at Site 1093 lies between the two others. This profile has a clear evaporative enrichment of chloride in several of the upper points. The shipboard data show a roughly linear

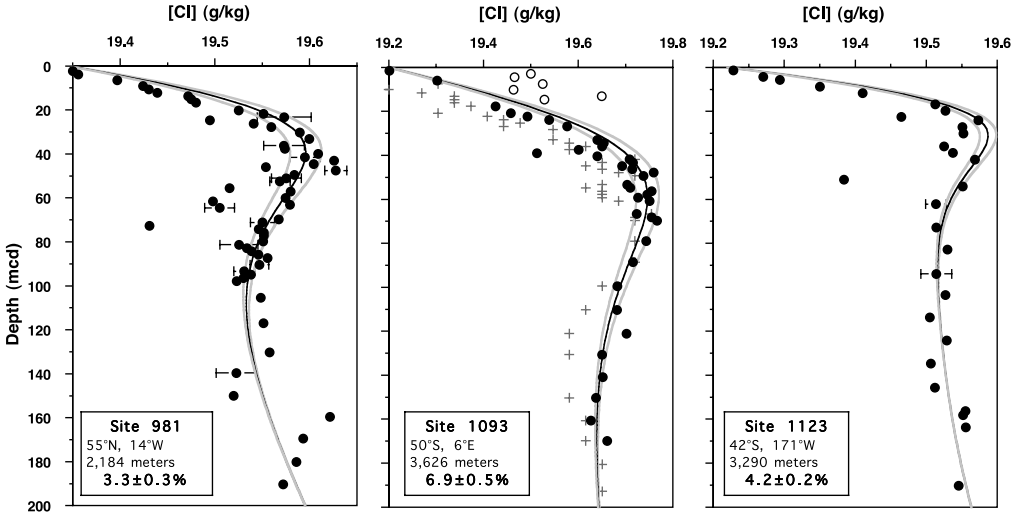

Fig. 11. Three profiles of [Cl] that show the effects of scatter in the data and model uncertainties. (Left) Site 981 from the Feni Drift. (Middle) Site 1093 from the Southern Ocean south of the Polar Front. Gray crosses are shipboard data that have larger individual uncertainties (not shown) but a consistent overall trend. Open circles are Caltech data that are clearly affected by evaporation post-shipboard measurement. (Right) Site 1123 from the Chatham Rise.

increase in [Cl] from the sediment–water interface to the LGM peak. Our Caltech data agree with the shipboard results everywhere except the upper part of the profile. Clearly these samples must have evaporated between sealing at sea and transport to our lab at Caltech. Even with the extreme care taken by the shipboard scientists, evaporation from glass ampoules occurs in some samples on virtually every ODP leg. However, outside of these sampling artifacts, Site 1093 has a relatively tight distribution of data. The scatter at the LGM peak translates into a larger relative uncertainty than at Site 1123 because D_{eff} is larger for the Southern Ocean site. At Site 1093 the depth of the [Cl] maximum is 15–20 m deeper than all other sites. A deeper peak in the profile demands a larger D_{eff} and therefore a modeled LGM salinity that is more sensitive to scatter in the data.

After all of this discussion of possible problems in the model, it is important to note one fact. The three most important contributions to our modeled uncertainties at a given site are scatter in the data, the choice of D_{eff}, and the shape of the bottom water boundary condition. However, the first-order signal of differences in LGM salinity between sites, that drives many of the conclusions in our previous work [12], is determined by the data, not the model. Our measured profile amplitudes, from LGM peak to modern bottom water value, are the most important parameters for setting the modeled LGM salinity. Our freshest site (1063) has the smallest measured change, while our saltiest site at the LGM (1093) has the largest amplitude in the data. As a rule of thumb, you could take the measured Δ[Cl] and multiply by two to get the LGM salinity change. The model is important for estimating uncertainties in this number, and getting better accuracy, but the principal signal is set by the data.

5.2. Using the pore fluid data without a model

In some sedimentary environments it is tempting to use the pore fluid data from the upper portions of the profile to constrain the LGM bottom water $\delta^{18}O$ and salinity without resorting to a sediment column model. With a very high sedimentation rate one might expect that the LGM bottom water signal could be 'trapped' at depth in the sediment before diffusion could work to dampen the signal [23]. But this interpretation misses the point that pore waters and sediments at the same core depth are not the same age. Diffusion and advection begin the instant the ocean is converted from bottom water to pore fluid. As long as porosity is interconnected, the $\delta^{18}O$ and [Cl] signals 'feel' the surface. This effect is demonstrated in Fig. 4B. For very large sedimentation rates (5 m/kyr) there is a 10-m change in the depth of the [Cl] maximum, but a very small change in the chloride concentration at that maximum. For a forcing that increases [Cl] by 1 g/kg there is only about 0.28 g/kg of signal left after 20 000 yr (Fig. 4B). Diffusion is still working to efficiently dampen the signal in this case.

Plots of [Cl] versus $\delta^{18}O$ for a single core show the trends in [Cl] and $\delta^{18}O$ of the local bottom waters through time, including the effects of diffusion and advection. Given that the deeper portions of the core are effected by both the bottom boundary conditions and reactions in the sediment, Duplessy et al. [24] suggested using the [Cl] vs. $\delta^{18}O$ trends in the upper sediment column to extrapolate to the LGM end-member without using a 1-D model. Using the data from Site 1063, they found larger values of $\delta^{18}O$ and [Cl] for the LGM than an earlier paper of ours that included a sediment diffusion model [11]. This extrapolation approach can lead to large errors in sediments where there are multiple processes occurring at different depths. An extrapolation of the [Cl] versus $\delta^{18}O$ plot for Site 981 is presented in Fig. 12. The modern and modeled LGM bottom water values are shown in dark gray and connected by a dashed line. Extrapolation lines from the data just above and just below the LGM peak in the data are shown as long black arrows. Duplessy et al. imply that the intersection of these two lines leads to a better representation of the LGM bottom water conditions. At Site 981 the upper trend line comes close to 'pointing' towards the modeled LGM answer, but is clearly affected by the fact that the trend near the peak LGM data is different from the trend near the core top. If we used just the shallow values,

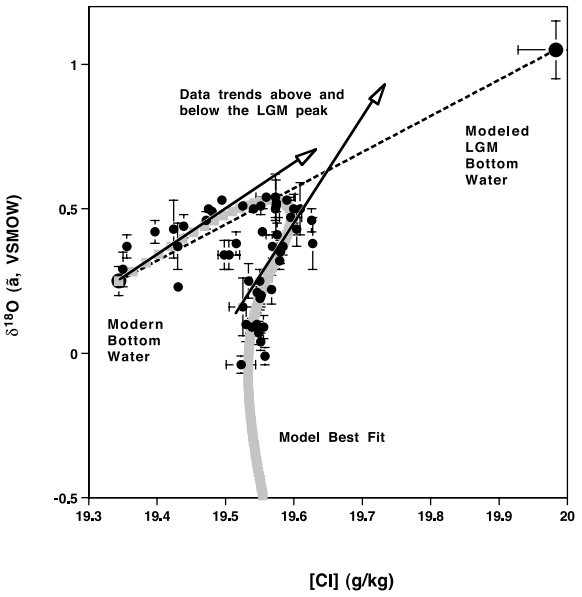

Fig. 12. Data from Site 981 plotted as $\delta^{18}O$ versus [Cl]. Extrapolations of the tracer versus tracer trends both above and below the LGM maximum do not intersect the model-reconstructed LGM bottom water values. Competing effects of Holocene [Cl] and $\delta^{18}O_{seawater}$ changes above the LGM maximum lead to heavy $\delta^{18}O$ values for a given [Cl] of the pore fluid. Separate deep-sediment boundary conditions for $\delta^{18}O$ and [Cl] lead to a grossly incorrect family of solutions for LGM bottom water based on extrapolating the trend below the LGM pore water peaks.

then the trend line would miss the modeled point by a large margin. Below the LGM data peak the trend line is determined by the separate shapes of $\delta^{18}O$ and [Cl] at depth in the core. The [Cl] 'turn around' discussed above is absent in the $\delta^{18}O$ data. This leads to a very steep line that cannot represent the LGM bottom water characteristics. These features lead to an intersection point that is clearly unrealistic for the LGM. While the separate evolution of $\delta^{18}O$ and [Cl] after the LGM is an interesting open question, a 1-D model is needed to accurately determine the LGM bottom water values.

6. Conclusions

Modeled salinities of the LGM bottom waters, as derived from pore fluid measurements, are insensitive to sedimentation rate, the choice of initial condition and porosity variations. Results are sensitive to the choice of diffusion coefficient, the shape of the bottom water forcing function and the scatter in the data. In general the data show an increase of about 1.5–2.0% from the sediment–water interface to the LGM peak at several 10s of meters depth. Measurement errors of around 0.05% (2σ) therefore translate into about a 30:1 signal-to-noise ratio, or better. Measured profiles are sometimes affected by both evaporation and freshwater addition during the sampling and storage prodedures, but these effects are readily apparent and can be eliminated from the modeled data set. Given the combined data and model uncertainties, the overall error at any individual site varies between 2 and 15% (or 0.1 and 0.5% where the mean ocean change is 3.5%). This is comparable with the uncertainties in $\delta^{18}O$ reconstructions [10].

Acknowledgements

During her stay at Caltech, Kate McIntyre collected many of the [Cl] profiles and provided many helpful comments on the modeling sensitivities. David Hodel, Chris Charles, Peggy Delaney, Alan Mix and all the inorganic chemists worked extremely hard to collect the pore fluid samples during ODP Legs 177 and 202. Reviews from L. Labeyrie, J. Lynch-Stieglitz and B. Boudreau greatly improved the manuscript. This work was supported by NSF Grant numbers OCE-0096814 to J.F.A. and OCE-0096909 to D.P.S.*[BARD]*

References

[1] J.-C. Duplessy, L. Labeyrie, A. Juillet-Leclerc, F. Maitre, J. Duprat, M. Sarnthein, Surface salinity reconstruction of the North Atlantic Ocean during the last glacial maximum, Oceanol. Acta 14 (1991) 311–324.

[2] J.C. Duplessy, L. Labeyrie, M. Paterne, S. Hovine, T. Fichefet, J. Duprat, M. Labracherie, High latitude deep water sources during the Last Glacial Maximum and the intensity of the global oceanic circulation, in: G. Wefer, W.H. Berger, G. Siedler, D.J. Webb (Eds.), The South Atlantic: Present and Past Circulation, Springer, Berlin, 1996, pp. 445–460.

[3] A. deVernal, J.L. Turon, J. Guiot, Dinoflagellate cyst distribution in high-latitude marine environments and quantitative reconstruction of sea-surface salinity, temperature, and seasonality, Can. J. Earth Sci. 31 (1994) 48–62.
[4] A. deVernal, C. HillaireMarcel, G. Bilodeau, Reduced meltwater outflow from the laurentide ice margin during the Younger Dryas, Nature 381 (1996) 774–777.
[5] Y. Rosenthal, E.A. Boyle, Factors controlling the fluoride content of planktonic foraminifera: An evaluation of its paleoceanographic applicability, Geochim. Cosmochim. Acta 57 (1993) 335–346.
[6] R.E. McDuff, The chemistry of interstitial waters, deep sea drilling project leg 86, DSDP Init. Rept. 86 (1985) 675–687.
[7] D.P. Schrag, D.J. DePaolo, Determination of del18O of seawater in the deep ocean during the Last Glacial Maximum, Paleoceanography 8 (1993) 1–6.
[8] D.P. Schrag, G. Hampt, D.W. Murry, Pore fluid constraints on the temperature and oxygen isotopic composition of the Glacial ocean, Science 272 (1996) 1930–1932.
[9] R.G. Fairbanks, R.K. Matthews, The marine oxygen isotope record in Pleistocene coral, Barbados, West Indies, Quat. Res. 10 (1978) 181–196.
[10] D.P. Schrag, J.F. Adkins, K. McIntyre, J. Alexander, D.A. Hodell, C.D. Charles, J.F. McManus, The oxygen isotopic composition of seawater during the Last Glacial Maximum, Quat. Sci. Rev. 21 (2002) 331–342.
[11] J.F. Adkins, D.P. Schrag, Pore fluid constraints on deep ocean temperature and salinity during the last glacial maximum, Geophys. Res. Lett. 28 (2001) 771–774.
[12] J.F. Adkins, K. McIntyre, D.P. Schrag, The salinity, temperature, and d18O of the glacial deep ocean, Science 298 (2002) 1769–1773.
[13] J.M. Gieskes, T. Gamo, H. Brumsack, Chemical methods for interstitial water analysis aboard JOIDES Resolution, ODP Tech. Note 15, 1991.
[14] B.P. Boudreau, Diagenetic Models and their Implementation, Springer, Berlin, 1997, 132 pp.
[15] R.A. Berner, Early Diagenesis: A Theoretical Approach, Princeton University Press, Princeton, NJ, 1980, 241 pp.
[16] J.B. Martin, Nonconservative behavior of Br/Cl ratios during alteration of volcaniclastic sediments, Geochim. Cosmochim. Acta 63 (1999) 383–391.
[17] R. Tiedemann, M. Sarnthein, N.J. Shackleton, Astronomic timescale for the Pliocene Atlantic Delta-O-18 and dust flux records of Ocean Drilling Program Site-659, Paleoceanography 9 (1994) 619–638.
[18] N.J. Shackleton, J. Imbrie, M.A. Hall, Oxygen and carbon isotope record of East Pacific core V19-30: implications for the formation of deep water in the late Pleistocene North Atlantic, Earth Planet. Sci. Lett. 65 (1983) 233–244.
[19] E. Bard, B. Hamelin, R.G. Fairbanks, A. Zindler, G. Mathieu, M. Arnold, U/Th and ^{14}C ages of corals from Barbados and their use for calibrating the ^{14}C time scale beyond 9000 years B.P., Nucl. Instrum. Methods B 52 (1990) 461–468.
[20] L.R. Edwards, W.J. Beck, G.S. Burr, D.J. Donahue, J.M.A. Chappell, A.L. Bloom, E.R.M. Druffel, F.W. Taylor, A large drop in atmospheric $^{14}C/^{12}C$ and reduced melting in the Younger Dryas, documented with ^{230}Th ages of corals, Science 260 (1993) 962–967.
[21] J. Chappell, N.J. Shackleton, Oxygen isotopes and sea level, Nature 324 (1986) 137–140.
[22] Y.H. Li, S. Gregory, Diffusion of ions in sea water and in deep-sea sediments, Geochim. Cosmochim. Acta 38 (1974) 703–714.
[23] S.J. Burns, M.A. Maslin, Composition and circulation of bottom water in the western Atlantic Ocean during the last glacial, based on pore-water analyses from the Amazon Fan, Geology 27 (1999) 1011–1014.
[24] J.-C. Duplessy, L. Labeyrie, C. Waelbroeck, Constraints on the ocean oxygen isotopic enrichment between the Last Glacial Maximum and the Holocene: paleoceanographic implications, Quat. Sci. Rev. 21 (2002) 315–330.